

# Nonpolar Side Chains Affect the Photochemical Redox Reactions of Copper(II)–Amino Acid Complexes in Aqueous Solutions

Chen-Jui Lin, Po-Yen Wang, Yi-Liang Lin, Sheng-Te Chang, Chao-Sheng Hsu, Shu-Pao Wu, and Chien-Hou Wu\*



Cite This: *ACS Omega* 2021, 6, 28194–28202



Read Online

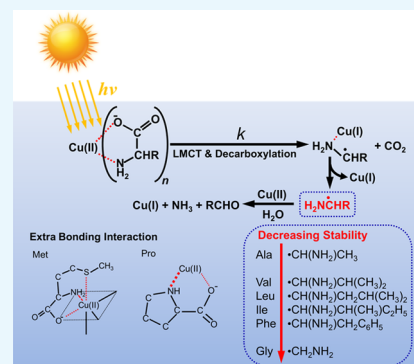
ACCESS |

Metrics & More

Article Recommendations

Supporting Information

**ABSTRACT:** Photochemical redox reactions of Cu(II) complexes of eight amino acid ligands (L) with nonpolar side chains have been systematically investigated in deaerated aqueous solutions. Under irradiation at 313 nm, the intramolecular carboxylate-to-Cu(II) charge transfer within Cu(II)–amino acid complexes leads to Cu(I) formation and the concomitant decomposition of amino acids. All amino acid systems studied here can produce ammonia and aldehydes except proline. For the 1:1 Cu(II) complex species (CuL), the Cu(I) quantum yields at 313 nm ( $\Phi_{\text{Cu(I),CuL}}$ ) vary by fivefold and in the sequence (0.10 M ionic strength at 25 °C) alanine (0.094) > valine (0.059), leucine (0.059), isoleucine (0.056), phenylalanine (0.057) > glycine (0.052) > methionine (0.032) > proline (0.019). This trend can be rationalized by considering the stability of the carbon-centered radicals and the efficient depopulation of the photoexcited state, both of which are dependent on the side-chain structure. For the 1:2 Cu(II) complex species (CuL<sub>2</sub>), the Cu(I) quantum yields exhibit a similar trend and are always less than those for CuL. The photoformation rates of ammonia, Cu(I), and aldehydes are in the ratio of 1:2.0 ± 0.2:0.7 ± 0.2, which supports the proposed mechanism. This study suggests that the direct phototransformation of Cu(II)–amino acid complexes may contribute to the bioavailable nitrogen for aquatic microorganisms and cause biological damage on cell surfaces in sunlit waters.



## 1. INTRODUCTION

The photochemical reactions of copper complexes with diverse organic ligands have received considerable attention in environmental, biological, and industrial processes.<sup>1–5</sup> The dissolved copper in natural waters is thought to form complexes with dissolved organic matter (DOM), mainly including amino, phenolic, alcoholic, ketonic, and carboxylic groups.<sup>6–11</sup> Plenty of photochemical redox reactions of copper complexes can occur in sunlit waters. Several investigations have shown that the sunlight-initiated photoredox reactions of DOM-bound Cu(II) species may have dramatic impacts on the speciation and biogeochemical cycling of copper, which can conversely alter the toxicity, bioavailability, and transport of copper in sunlit waters.<sup>12–15</sup>

The photochemical release of ammonium from dissolved organic matter (DOM) is an important source of bioavailable nitrogen in N-limited aquatic ecosystems and the relative abundance of individual amino acids in the DOM pool has been shown to have a strong correlation with the degradation stage and the bioavailability of DOM.<sup>16–21</sup> Amino acids are exuded by phytoplankton in the ocean, but the chemical structure of the dissolved combined amino acids remains poorly understood.<sup>22</sup> Several studies state that glycine is most frequently identified as the most abundant amino acid in diverse environmental scenarios.<sup>23,24</sup> Phytochelutins, metal chelators produced by marine diatoms upon exposure to

metals, are small polypeptides containing the amino acid glutamate, cysteine, and glycine.<sup>25,26</sup> Algae play a significant role in the uptake and regulation of copper in natural waters by their surfaces (i.e., membranes and cell walls) for copper binding. In diatoms, these walls comprise a silica frustule encased in an organic coating, which is enriched in the amino acid glycine, serine, and threonine.<sup>27</sup> Dissolved free and combined amino acids are ubiquitous in natural waters, and the photochemical degradation of amino acids through either direct or indirect photolysis has been assessed in sunlit waters.<sup>28–30</sup> Under solar irradiation, only tyrosine and tryptophan were subject to direct photodegradation. The addition of DOM, an important photosensitizer, can greatly enhance the indirect photodegradation of histidine, methionine, tyrosine, and tryptophan. Although the four amino acids are susceptible to photochemical degradation, the remaining common amino acids seem to be photostable in natural waters. This implies that the amino acid structure plays an important role in photoreactivity.

Received: August 9, 2021

Accepted: October 1, 2021

Published: October 13, 2021



**Table 1. Equilibrium Formation Constants, Components, and Their Stoichiometric Coefficients for the Calculated Cu(II) Complex Species<sup>a</sup>**

species <sup>b</sup>	components										equilib. constant		notes
	Cu <sup>2+</sup>	H <sup>+</sup>	Gly <sup>-</sup>	Ala <sup>-</sup>	Val <sup>-</sup>	Leu <sup>-</sup>	Ile <sup>-</sup>	Pro <sup>-</sup>	Phe <sup>-</sup>	Met <sup>-</sup>	log <sub>10</sub> (β)		
Cu(Gly) <sup>+</sup>	1		1								8.19		
Cu(Gly) <sub>2</sub> <sup>0</sup>	1		2								15.10		
Cu(Ala) <sup>+</sup>	1			1							8.11		
Cu(Ala) <sub>2</sub> <sup>0</sup>	1			2							14.90		
Cu(Val) <sup>+</sup>	1				1						8.10		
Cu(Val) <sub>2</sub> <sup>0</sup>	1				2						14.97		
Cu(HVal) <sup>2+</sup>	1	1			1						10.50	0.15, 37°	
Cu(Val)(HVal) <sup>+</sup>	1	1			2						18.74	0.15, 37°	
Cu(Leu) <sup>+</sup>	1					1					8.14		
Cu(Leu) <sub>2</sub> <sup>0</sup>	1					2					15.00		
Cu(HLeu) <sup>2+</sup>	1	1				1					11.66	0.15, 37°	
Cu(Leu)(HLeu) <sup>+</sup>	1	1				2					19.60	0.15, 37°	
Cu(Ile) <sup>+</sup>	1						1				8.14		
Cu(Ile) <sub>2</sub> <sup>0</sup>	1						2				15.02		
Cu(OH)(Ile) <sup>0</sup>	1	-1					1				0.66	0.15, 37°	
Cu(Pro) <sup>+</sup>	1							1			8.84		
Cu(Pro) <sub>2</sub> <sup>0</sup>	1							2			16.36		
Cu(HPro) <sup>2+</sup>	1	1						1			11.41	0.15, 37°	
Cu(Pro)(HPro) <sup>+</sup>	1	1						2			20.45	0.15, 37°	
Cu(Phe) <sup>+</sup>	1								1		7.77		
Cu(Phe) <sub>2</sub> <sup>0</sup>	1								2		14.65		
Cu(Met) <sup>+</sup>	1									1	7.86		
Cu(Met) <sub>2</sub> <sup>0</sup>	1									2	14.51		

<sup>a</sup>All equilibrium formation constants (β) are for 1.0 atm, 25 °C, and ionic strength *I* = 0.10 M (except where noted otherwise). Equilibrium formation constants for all inorganic Cu(II) species are taken into consideration and details of the definition of symbols are described elsewhere.<sup>36</sup> The p*K*<sub>a</sub> values of the species used here are Gly (2.33, 9.57), Ala (2.33, 9.71), Val (2.26, 9.50), Leu (2.32, 9.56), Ile (2.27, 9.59), Pro (1.90, 10.47), Phe (2.18, 9.09), Met (2.16, 9.08), H<sub>3</sub>PO<sub>4</sub> (1.92, 6.71, 11.65), and H<sub>2</sub>CO<sub>3</sub><sup>\*</sup> (6.13, 9.88), where H<sub>2</sub>CO<sub>3</sub><sup>\*</sup> ≡ H<sub>2</sub>CO<sub>3</sub>(aq) + CO<sub>2</sub>(aq) (25 °C, *I* = 0.10 M, and 1.0 atm). Log<sub>10</sub>(*K*<sub>w</sub>) = -13.78 for *K*<sub>w</sub> = [H<sup>+</sup>][OH<sup>-</sup>] (25 °C, *I* = 0.10 M, and 1.0 atm). <sup>b</sup>HVal<sup>0</sup>, HLeu<sup>0</sup>, and HPro<sup>0</sup> stand for the monoprotonated forms of amino acids.

The kinetics of the photolysis of Cu(II)–amino acid complexes have been very intensively investigated during the last four decades.<sup>1,31–35</sup> The ligand-to-metal charge transfer (LMCT) irradiations of Cu(II) complexes with glycine and alanine lead to Cu(I) formation and induce decarboxylation of the ligand to produce CO<sub>2</sub>, NH<sub>3</sub>, and HCHO and CH<sub>3</sub>CHO, respectively.<sup>34</sup> Previous studies were generally conducted to measure the average photoproduct yields or the quantum yields for CuL<sub>2</sub>, where CuL<sub>2</sub> existed dominantly in the conditions. Very few quantum yields for individual Cu(II)–amino acid complex species have been conducted. Therefore, a systematic assessment of the effect of amino acid ligand structure on individual quantum yields is important to evaluate the photochemical behavior of Cu(II)–amino acid complexes in natural waters. To precisely determine the Cu(I) quantum yield, the experiments should be performed in the absence of oxygen. In this study, we extend our previous work to include Cu(II) complexes of amino acids with a series of nonpolar side chains involving methionine (Met), glycine (Gly), alanine (Ala), valine (Val), leucine (Leu), isoleucine (Ile), phenylalanine (Phe), and proline (Pro) in deaerated aqueous solution.<sup>36</sup> The quantum yields of photoproducts for individual Cu(II)–amino acid complex species would be characterized and the effects of side-chain structure and of the Cu(II)–amino acid complex stoichiometry on their quantum yields clarified. The results obtained in this study are considered to be valuable for the understanding of the LMCT mechanisms of Cu(II)–amino acid complexes on cell surfaces for biological

damage, Cu(II)–bacteria complexes for water disinfection, and Cu(II)–DOM complexes for the inhibition of triplet sensitized phototransformation.<sup>37–40</sup>

## 2. RESULTS AND DISCUSSION

**2.1. Characterization of Cu(II) Complexes.** Table 1 summarizes Cu(II) complexes with different amino acids and their corresponding p*K*<sub>a</sub> values and equilibrium formation constants. Nonpolar side-chain amino acids show strong complexation ability with Cu(II) through the amino nitrogen and carboxylate oxygen atoms and are capable of establishing planar mono- and bis-complexes (CuL and CuL<sub>2</sub>), which are the major species throughout the experimental ranges studied here. The Cu(II) speciation can be calculated from equilibrium computations with reliable equilibrium formation constants.<sup>41,42</sup>

From equilibrium speciation calculations for the molar absorbance and photochemical experiments of each Cu(II)–amino acid solution, the Cu(II) complex species CuL and CuL<sub>2</sub> constituted at least 86% for all but two experiments for leucine and proline. In most experimental conditions, inorganic Cu(II) species were kept at a minor fraction smaller than 10% of the total Cu(II) concentration.

The total rate of the Cu(I) photoformation for a Cu(II)–amino acid complex is dependent on two important factors: its molar absorptivity and quantum yield at 313 nm. Molar absorptivities for individual species at a given wavelength can be expressed as

$$\varepsilon_{\text{Cu(II)}} = \sum_i (\varepsilon_i f_i) \quad (1)$$

where  $\varepsilon_{\text{Cu(II)}}$  is the experimental Cu(II)-based molar absorptivity ( $\text{M}^{-1} \text{cm}^{-1}$ ),  $\varepsilon_i$  is the molar absorptivity of individual Cu(II) complexes,  $\varepsilon_{\text{in}}$  is an average value for all inorganic Cu(II) species,  $f_i$  is the fraction of the total copper present as the  $i$ th Cu(II) complex species (e.g.,  $f_{\text{CuL}}$  and  $f_{\text{CuL}_2}$ ), and  $f_{\text{in}}$  is the fraction of all forms of inorganic Cu(II) species.<sup>43</sup> As an example, Figure 1 shows the typical UV-vis absorption

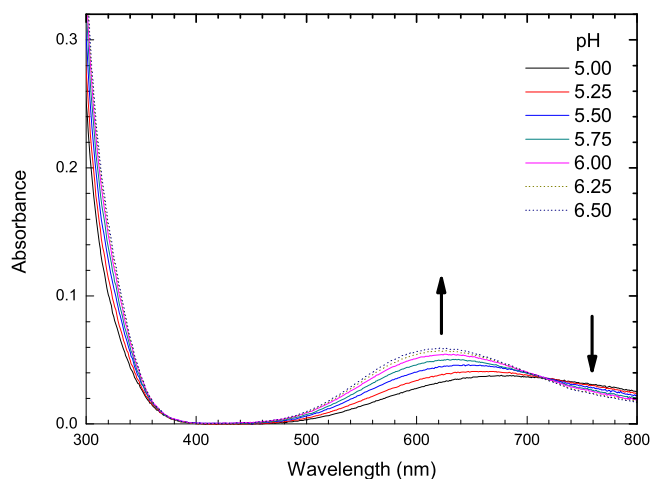


**Figure 1.** UV-vis spectra of Cu(II)/Met complexes recorded as a function of pH (optical path length 5.00 cm,  $[\text{Cu(II)}]_{\text{T}} = 200 \mu\text{M}$ ,  $[\text{Met}]_{\text{T}} = 2.0 \text{ mM}$ , 100  $\mu\text{M}$  phosphate buffer, and 0.1 M NaCl).

spectra of Cu(II)/Met systems. Absorbance in the UV region below 400 nm is attributed to LMCT, which can initiate the photochemical redox reactions of Cu(II)/Met complexes.

For the absorbance measurements of Cu(II)/Met systems at 313 nm, 21 data points were measured over a wide range of solution conditions (details in the Supporting Information). Figure 2 shows the correlation between the experimental quantity and the calculated fraction of Cu(II) speciation ( $f_{\text{CuL}}$ ). The best-fit values for the molar absorptivities of CuL and CuL<sub>2</sub> ( $\varepsilon_{\text{CuL}}$  and  $\varepsilon_{\text{CuL}_2}$ ) were determined from a

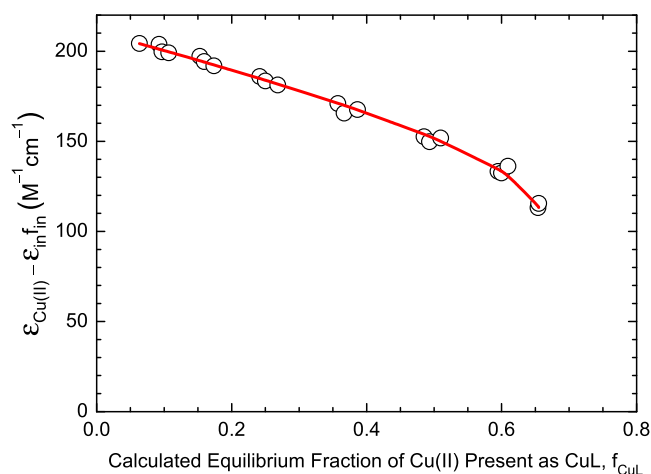


**Figure 2.** Experimental molar absorptivities of Cu(II)/Met complexes at 313 nm as a function of the calculated equilibrium fraction of Cu(II) speciation ( $f_{\text{CuL}}$ ) over a wide range of solution conditions.

multivariate linear regression of eq 1. In this case, the best-fit curve shown here is not a straight line as it would be if  $f_{\text{in}}$  was negligible. The fitting result indicates that the molar absorptivity for CuL<sub>2</sub> ( $211 \text{ M}^{-1} \text{cm}^{-1}$ ) is higher than that for CuL ( $108 \text{ M}^{-1} \text{cm}^{-1}$ ) in Cu(II)/Met systems. Table 2 summarizes the molar absorptivities of individual complex species for each Cu(II)-amino acid system at 313 nm. Those that exist at an isosbestic point around 300 nm including Gly, Ala, Val, Leu, and Ile have higher molar absorptivities (at 313 nm) for CuL than that for CuL<sub>2</sub>. As listed in Table 2, the molar absorptivity increases with the increasing side-chain alkyl groups. The hyperchromic effect could be ascribed to the formation of a strong covalent-bonding interaction between amino acid and Cu(II), which is related to the electron density donating tendencies of the ligand. It is also noteworthy that Met and Pro have relatively greater molar absorptivities at 313 nm. From a comparison of the spectra in the UV region with those of other amino acids, Cu(II)/Met complexes exhibited a broader band below 400 nm, shown in Figure 1, and the enhancement of the absorption intensity could be attributed to the thioether group of Met. The strong Cu-S interaction has been well-established in blue copper proteins.<sup>44,45</sup> Unlike the primary amino acids, Pro has a secondary amine in the strained pyrrolidine ring, which results in a stronger Cu-N bond and stability constant enhancement as listed in Table 1. Therefore, Cu(II)/Pro has the highest molar absorptivity among amino acids in Table 2.

## 2.2. Photochemical Behavior of Cu(II) Complexes.

The kinetic behavior of the Cu(I) photoformation from the Cu(II) complexes has been well-established. If the total absorbance is lower than 0.042 and the transformation of Cu(II) to Cu(I) is less than 10% of the total Cu(II) concentration, the total initial rate of the Cu(I) photoformation can be determined as

$$\begin{aligned} R_{\text{Cu(I)}}^0 &= [\ln(10)]I_0 D \Phi_{\text{Cu(I)}} \varepsilon_{\text{Cu(II)}} [\text{Cu(II)}]_{\text{T}} \\ &= j_{\text{Cu(I)}} [\text{Cu(II)}]_{\text{T}} \end{aligned} \quad (2)$$

where  $I_0$  is the volume-averaged incident actinic flux ( $\text{einstein L}^{-1} \text{s}^{-1}$ ) determined by 2-NB chemical actinometry,  $D$  is the optical path length (cm),  $j_{\text{Cu(I)}}$  is the apparent first-order rate constant for the Cu(I) photoformation ( $\text{s}^{-1}$ ), and  $\Phi_{\text{Cu(I)}}$  is the experimental Cu(I) quantum yield (mole  $\text{einstein}^{-1}$ ).<sup>43</sup> Figure 3 shows a series of kinetic plots of the Cu(I) photoformation for seven Cu(II)-amino acid systems. The slope of this plot obeys the first-order rate and reveals a good linear relationship calculated from eq 2. The linear regression  $r^2$  values for the first-order kinetic plots of this type were  $\geq 0.98$  for all Cu(II)-amino acid systems (92 experiments) but five experiments did not qualify.

Since the sum of the initial rates of the Cu(I) photoformation for individual Cu(II) complex species gives the total Cu(I) photoformation rate in the Cu(II)-amino acid system, the Cu(I) quantum yields for individual Cu(II) complex species can be expressed as

$$\Phi_{\text{Cu(I)}} \varepsilon_{\text{Cu(II)}} = \sum_i (\Phi_{\text{Cu(I),i}} \varepsilon_i f_i) \quad (3)$$

where the quantity  $\Phi_{\text{Cu(I)}} \varepsilon_{\text{Cu(II)}}$  is an experimental value from eq 2 and the individual Cu(I) quantum yields (mole  $\text{einstein}^{-1}$ ) includes  $\Phi_{\text{Cu(I),CuL}}$  for CuL,  $\Phi_{\text{Cu(I),CuL}_2}$  for CuL<sub>2</sub>, and  $\Phi_{\text{Cu(I),in}}$  for the average of all inorganic Cu(II) species.<sup>43</sup>

**Table 2. Summary of Molar Absorptivities ( $M^{-1} \text{ cm}^{-1}$ ) and Cu(I) Quantum Yields (mole einstein $^{-1}$ ) for the Individual Cu(II) Complex Species at 313 nm<sup>a</sup>**

ligand	$\epsilon_{\text{CuL}}$	$\epsilon_{\text{CuL}_2}$	$\epsilon_{\text{CuL}}/\epsilon_{\text{CuL}_2}$	$\Phi_{\text{Cu(I),CuL}}$	$\Phi_{\text{Cu(I),CuL}_2}$	$\Phi_{\text{Cu(I),CuL}}/\Phi_{\text{Cu(I),CuL}_2}$	$(\epsilon_{\text{CuL}})(\Phi_{\text{Cu(I),CuL}})$	$(\epsilon_{\text{CuL}_2})(\Phi_{\text{Cu(I),CuL}_2})$
Gly	$30 \pm 2$	$20 \pm 1$	1.5	$0.052 \pm 0.014$	$0.033 \pm 0.013$	1.6	$1.56 \pm 0.40$	$0.65 \pm 0.25$
Ala <sup>b</sup>	$40 \pm 4$	$29 \pm 2$	1.4	$0.094 \pm 0.014$	$0.064 \pm 0.012$	1.5	$3.74 \pm 0.43$	$1.87 \pm 0.32$
Val	$66 \pm 1$	$58 \pm 1$	1.1	$0.059 \pm 0.012$	$0.039 \pm 0.008$	1.5	$3.88 \pm 0.76$	$2.24 \pm 0.49$
Leu	$62 \pm 4$	$51 \pm 3$	1.2	$0.059 \pm 0.017$	$0.043 \pm 0.018$	1.4	$3.66 \pm 1.05$	$2.18 \pm 0.91$
Ile	$71 \pm 4$	$64 \pm 2$	1.1	$0.056 \pm 0.006$	$0.046 \pm 0.005$	1.2	$4.00 \pm 0.39$	$2.97 \pm 0.30$
Phe	$74 \pm 2$	$85 \pm 1$	0.9	$0.057 \pm 0.016$	$0.046 \pm 0.007$	1.2	$4.19 \pm 1.17$	$3.90 \pm 0.63$
Met	$108 \pm 7$	$211 \pm 4$	0.5	$0.032 \pm 0.008$	$0.016 \pm 0.003$	2.0	$3.46 \pm 0.84$	$3.45 \pm 0.56$
Pro	$145 \pm 5$	$250 \pm 3$	0.6	$0.019 \pm 0.005$	$0.011 \pm 0.002$	1.7	$2.81 \pm 0.67$	$2.78 \pm 0.52$

<sup>a</sup>Best value  $\pm 1$  SD for 0.10 M ionic strength (NaCl) at 25 °C. The wide range of solution conditions is provided in the Supporting Information.

<sup>b</sup>Reference 36.

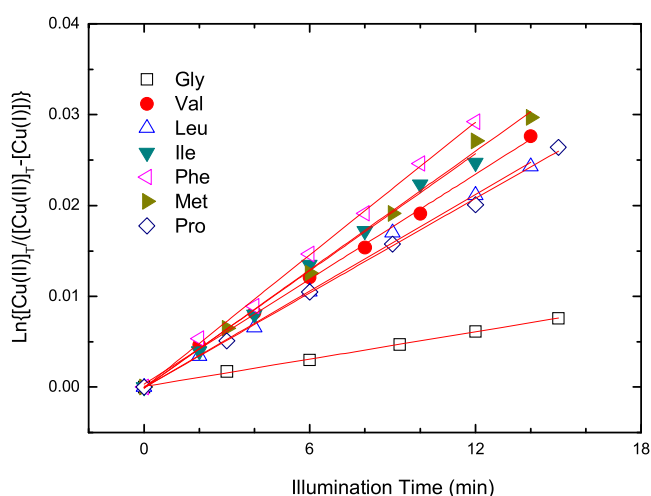


**Figure 3.** Correlation of Cu(I) photoformation at 313 nm with illumination time. Cu(II)–amino acid systems with  $[\text{Cu(II)}]_{\text{T}} = 50 \mu\text{M}$ ,  $[\text{amino acid}]_{\text{T}} = 2.0 \text{ mM}$ , and  $\text{pH} = 6.00$  (100  $\mu\text{M}$  phosphate buffer and 0.1 M NaCl).

The initial photoformation rates of ammonia and aldehydes under previous conditions show similar expression forms as in eq 3. As an example, Figure 4 displays the relationship between

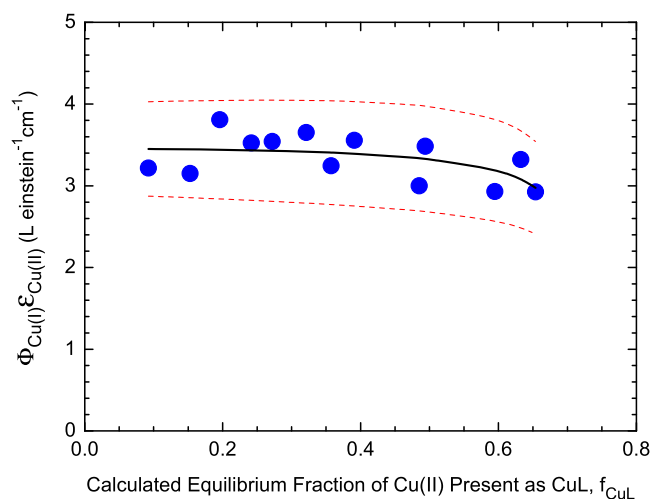


**Figure 4.** Measured photochemical parameters of Cu(II)/Met complexes as a function of the calculated fraction of Cu(II) speciation ( $f_{\text{CuL}}$ ) over a wide range of solution conditions. The dashed red lines indicate the 95% confidence interval.

the photochemical parameters ( $\Phi_{\text{Cu(I)}}\epsilon_{\text{Cu(II)}}$ ) and the calculated fraction of Cu(II) speciation ( $f_{\text{CuL}}$ ) for Cu(II)/Met systems. The best-fit values were determined from a multivariate linear regression of eq 3. These results demonstrate that the rate of the Cu(I) photoformation is mainly governed by the Cu(II) speciation (see the Supporting Information for the remaining amino acid systems). The Cu(I) quantum yields of individual complexes for each Cu(II)–amino acid system studied here are independent of the solution composition, as presented in Table 2. The observed reactivity of the Cu(I) quantum yields varies by fivefold for CuL and by sixfold for CuL<sub>2</sub>. It is noteworthy that the Cu(I) quantum yields for Cu(II)–amino acid complexes are lower than those for Cu(II)–dicarboxylate complexes due to the efficient depopulation of the photoexcited state by the strong Cu–N bond.<sup>46,47</sup>

**2.3. Effect of Amino Acid Side-Chain Structure on the Quantum Yield.** Because Cu(II) complexes of amino acids with different nonpolar side chains have a similar coordination structure involving stable five-membered chelates through the  $\alpha$ -amine and carboxylate moieties, a proposed mechanism for the photochemical redox reaction of Cu(II)–amino acid complexes could be illustrated in Figure 5. Briefly, this mechanism involves an efficient LMCT process by decarboxylation, photoformation of Cu(I) and carbon-centered radicals, and subsequent reaction of the carbon-centered radicals to form Cu(I), NH<sub>3</sub>, and aldehydes. When the steady-state approximation is applied to the intermediates  $[\text{Cu(I)-NH}_2\dot{\text{C}}\text{HR}]$  and  $[\text{NH}_2\dot{\text{C}}\text{HR}]$ , the decarboxylation rate of the direct photochemical process is equal to the oxidation rate of carbon-centered radicals with Cu(II) complexes. Based on this assumption, the irradiations of Cu(II)/Gly and Ala complexes induce decarboxylation of the ligands to carbon dioxide, ammonia, and aldehydes in the ratio of 2:1:1 in the previous final product analysis.<sup>34,36</sup> As listed in Table 3, the results are similar to those in the Cu(II)/Val, Leu, Ile, Phe, and Met systems giving the formation rates of Cu(I), NH<sub>3</sub>, and aldehydes in the ratio of  $2.0 \pm 0.2:1:0.7 \pm 0.2$ . Neither ammonia nor aldehyde was detected in the Cu(II)/Pro system probably due to the formation of secondary amines.

In Figure 5, the trans form of the 1:2 complex (CuL<sub>2</sub>) is depicted according to the study that about 60% of the complexes were present as the trans isomer in aqueous solutions with 0.10 M KNO<sub>3</sub> as the background.<sup>48</sup> The previous study indicates that a cis–trans isomer equilibrium occurs rapidly in aqueous solutions and the cis–trans ratio is little affected by the nature of the side chain. It is worth noting that the addition of a salt background has an influence on the

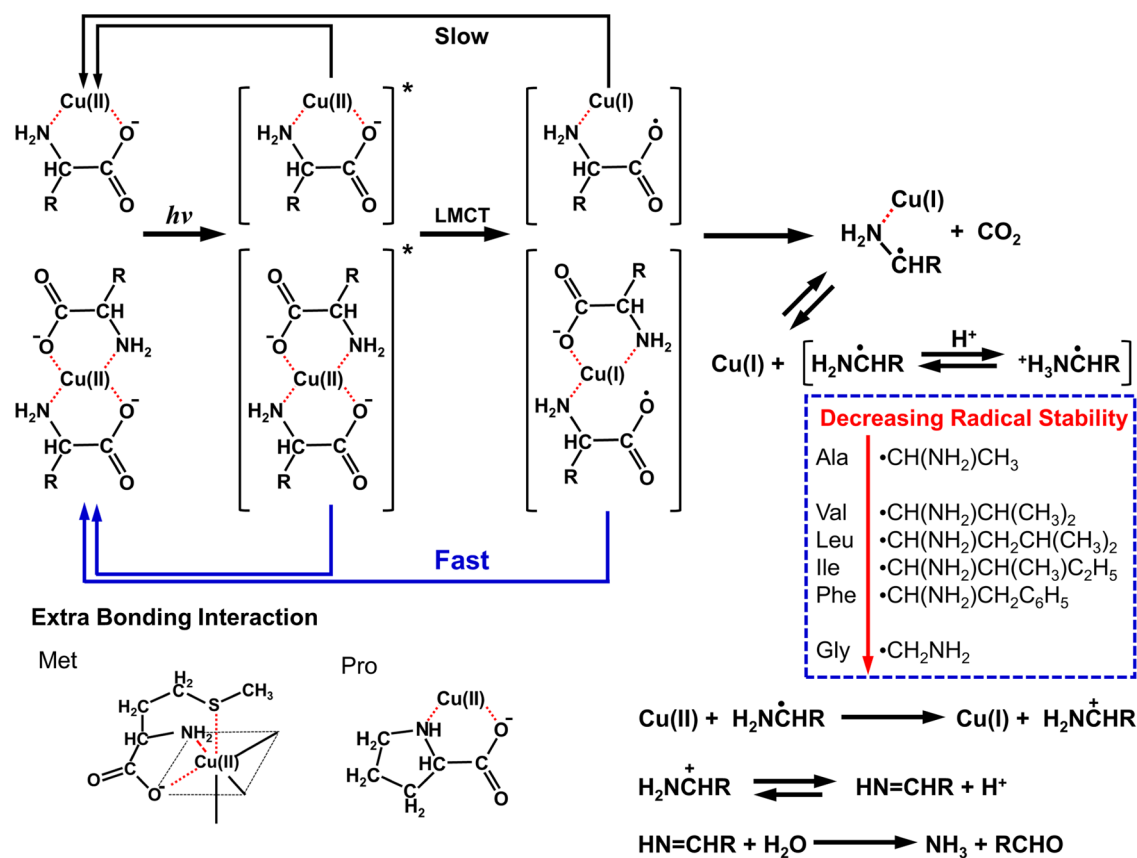


**Figure 5.** Proposed mechanism for the photochemical redox reaction of Cu(II)–amino acid complexes. The amino acids studied differ in the side-chain R.

**Table 3. Summary of the Ratio of the Total Initial Photoformation Rates of Cu(I) to Ammonia and Aldehydes for Cu(II)–Amino Acid Complexes at 313 nm<sup>a</sup>**

	Gly	Ala <sup>b</sup>	Val	Leu	Ile	Phe	Met	Pro
$R_{\text{Cu(I)}}^0/R_{\text{NH}_3}^0$	1.70	1.74	2.15	2.18	2.07	1.90	2.09	ND <sup>c</sup>
$R_{\text{Cu(I)}}^0/R_{\text{RCHO}}^0$	1.62	2.58	2.56	3.17	3.02	2.43	1.89	ND

<sup>a</sup>The wide range of solution conditions is provided in Table S1. <sup>b</sup>Reference 36. <sup>c</sup>ND: not detected.

cis–trans isomer equilibrium in favor of the formation of the cis isomer.<sup>49</sup>

As can be seen in Table 2, the Cu(I) quantum yields vary in the order Ala > Val, Leu, Ile, Phe > Gly > Met > Pro. The rate of decarboxylation is strongly dependent upon the stability of the carbon-centered radicals, which is expected to alter the overall quantum yield of the photoproducts. The textbook-level view of radical stability follows the order tertiary > secondary > primary > methyl, which results from the modestly stabilizing hyperconjugation with an adjacent alkyl group.<sup>50</sup> The aminomethyl radical •CH<sub>2</sub>NH<sub>2</sub>, derived from decarboxylation of the glycine radical, is expected to be relatively less stable due to its lower ordinality. However, it is quite challenging to predict the stability of the same primary radicals that are derived from decarboxylation of alanine, valine, leucine, isoleucine, and phenylalanine.

The thermodynamic stability of carbon-centered radicals has various types of definitions, and one of the most used definitions is based on isodesmic hydrogen-transfer reactions where the reaction enthalpy of this process is often expressed as the radical stabilization energy (RSE).<sup>51</sup> The RSE values are commonly negative for radicals, which are relatively more

stable than the methyl radical •CH<sub>3</sub>. Thus, as a reference system, the RSE of the methyl radical •CH<sub>3</sub> is 0 kJ mol<sup>-1</sup>. All RSE values used in this article are provided by Hioe and Zipse, who used the G3(MP2)-RAD method. This method has been successfully applied to estimate the stability of the radical species.<sup>51–53</sup> The RSE values for the ethyl radical •CH<sub>2</sub>CH<sub>3</sub>, *n*-propyl radical •CH<sub>2</sub>CH<sub>2</sub>CH<sub>3</sub>, *n*-butyl radical •CH<sub>2</sub>CH<sub>2</sub>CH<sub>2</sub>CH<sub>3</sub>, 2-methylprop-1-yl radical •CH<sub>2</sub>CH(CH<sub>3</sub>)<sub>2</sub>, and 2-phenyleth-1-yl radical •CH<sub>2</sub>CH<sub>2</sub>C<sub>6</sub>H<sub>5</sub> are –13.5, –12.2, –12.2, –10.6, and –10.4 kJ mol<sup>-1</sup> relative to the methyl radical •CH<sub>3</sub>, respectively. Increasing the size of the attached alkyl group may result in a small but notable reduction in radical stability. This trend implies that the hyperconjugative effect through the interaction of the unpaired spin with adjacent bonds is stronger than the inductive electron withdrawal effect of the alkyl groups. Noticeably, the remote  $\pi$ -orbitals of the aromatic ring do not lead to more efficient stabilization. On the other hand, the stability of alkyl radicals could be greatly enhanced through a lone-pair donation. Amino-substituted radicals appear to be quite important in enhancing the stability of aminomethyl radical •CH<sub>2</sub>NH<sub>2</sub> (RSE = –44.9 kJ mol<sup>-1</sup>) and 1-aminoethyl radical

$\bullet\text{CHNH}_2\text{CH}_3$  (RSE =  $-49.9 \text{ kJ mol}^{-1}$ ), both of which are much more stable than the methyl radical  $\bullet\text{CH}_3$  and the ethyl radical  $\bullet\text{CH}_2\text{CH}_3$ , respectively. The experimentally measured RSE value for  $\bullet\text{CHNH}_2\text{CH}_3$  is  $-62.3 \text{ kJ mol}^{-1}$ , which leads to much larger stabilization energy and further confirms that the carbon-centered radical derived from the decarboxylation of alanine is the most stable one among the eight amino acids.<sup>54</sup> Although the interplay of the amino group attached to the radical center results in much more stable carbon-centered radicals, the stability of amino-substituted radicals follows the same trend as the radicals listed above. Therefore, the stability of the carbon-centered radicals follows the trend  $\bullet\text{CH}(\text{NH}_2)\text{CH}_3 > \bullet\text{CH}(\text{NH}_2)\text{CH}(\text{CH}_3)_2 \sim \bullet\text{CH}(\text{NH}_2)\text{CH}_2\text{CH}(\text{CH}_3)_2 \sim \bullet\text{CH}(\text{NH}_2)\text{CH}(\text{CH}_3)\text{C}_2\text{H}_5 \sim \bullet\text{CH}(\text{NH}_2)\text{CH}_2\text{C}_6\text{H}_5 > \bullet\text{CH}_2\text{NH}_2$ , which are derived from decarboxylation of the Ala, Val, Leu, Ile, Phe, and Gly radicals, respectively. Figure 6

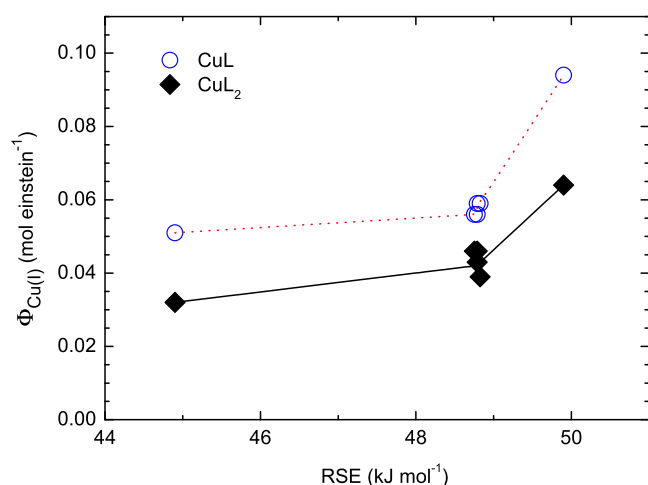


**Figure 6.** Correlation between the individual Cu(I) quantum yield and RSE of relative ligands.

shows the correlation between RSE and quantum yield. The orders in Cu(I) quantum yields of Cu(II)–amino acid complexes are amazingly the same as the trend of the stability of the carbon-centered radicals.

Cu(II)–amino acid complexes involve a common five-membered chelate ring by N,O-chelation as shown in Figure 5, but Met and Pro systems have a little bit different binding properties with Cu(II), which result in a dramatic change of the Cu(I) quantum yields. The thioether group of Met could interact with Cu(II) to form an additional Cu–S bond, although the interaction is weak and does not contribute importantly to the complex stability. The strain of the secondary N-donor of Pro could interact with Cu(II) to form a much stronger Cu–N bond, and this interaction does enhance the stability constant as listed in Table 1. Both Cu–S and stronger Cu–N bonds could provide an efficient pathway for the nonradiative electronic relaxation of the LMCT state. Therefore, in addition to the stability of the carbon-centered radicals, the efficient depopulation of the photoexcited state is also a significant factor affecting the Cu(I) quantum yields for Met and Pro systems.

**2.4. Photoreaction Rate Constants in Sunlight.** The photoreaction rate constants for the photoformation of Cu(I) from Cu(II)–amino acid complexes in sunlight (solar zenith angle = 30°) are shown in Table 4 and the half-lives vary by a factor of 9 between 10 and 93 h. The photoreactivity of

**Table 4. Summary of Photoreaction Rate Constants in Sunlight**

ligand	$j_{\text{CuL} \rightarrow \text{Cu(I)}}$ , sec <sup>-1</sup>	half-life (h)	$j_{\text{CuL}_2 \rightarrow \text{Cu(I)}}$ , sec <sup>-1</sup>	half-life (h)
Gly	$4.45 \times 10^{-6}$	43	$2.06 \times 10^{-6}$	93
Ala	$1.17 \times 10^{-5}$	16	$5.35 \times 10^{-6}$	36
Val	$1.06 \times 10^{-5}$	18	$8.41 \times 10^{-6}$	23
Leu	$1.43 \times 10^{-5}$	13	$6.84 \times 10^{-6}$	28
Ile	$1.09 \times 10^{-5}$	18	$8.18 \times 10^{-6}$	24
Phe	$1.33 \times 10^{-5}$	14	$1.18 \times 10^{-5}$	16
Met	$1.73 \times 10^{-5}$	11	$1.93 \times 10^{-5}$	10
Pro	$9.46 \times 10^{-6}$	20	$7.61 \times 10^{-6}$	25

Cu(II)–amino acid complexes in sunlight is dependent upon both their quantum yields and molar absorptivities. Therefore, although the Cu(II)/Ala complex reacts with the highest quantum yield among the systems studied, the shortest half-life is calculated for the Cu(II)/Met complex due to its greater molar absorptivity. It implies that the direct phototransformation of Cu(II)/Met complexes needs to be considered in sunlit waters. Yet, a general inverse relationship between abundances of amino acids and thermodynamic free energies for the synthesis of each amino acid has been proposed.<sup>55</sup> The longest half-life for the Cu(II)/Gly complex might be reflective of its most abundance in aquatic environments. Furthermore, most CuL complexes have higher photoactivities than CuL<sub>2</sub> complexes, which could be ascribed to the Cu(II)-stabilizing effect of the second ligand, shown in Table 2. Generally, CuL is a predominant species in natural waters where copper is typically found in nanomolar concentrations. This implies that the photoreactivity of Cu(II)–amino acid complexes is underestimated if the evaluation is based on previous studies where CuL<sub>2</sub> is the major species. In the presence of oxygen, the photoreduced Cu(I) can easily react with oxygen to reform Cu(II).<sup>56</sup> Nevertheless, the photoformation of Cu(I) observed in deaerated solution is still related to the photodegradation of amino acids in the solution containing oxygen. The photoformation rate constants of NH<sub>3</sub> and aldehydes in air-saturated solutions could be approximately estimated from Table 4, with related values divided by 2. Because Cu(II) can become an effective catalyst for the degradation of amino acids in the presence of oxygen, the calculated photoformation rate constants of NH<sub>3</sub> and aldehydes would be lower bounds in sunlit waters.

The degradation of amino acids may significantly influence the cycling of carbon and nitrogen in the upper column water. In the presence of oxygen, the photoreduced Cu(I) can easily react with oxygen to reform Cu(II); thus, the photocatalytic redox cycle of copper can enhance the degradation of amino acids. Our preliminary data show that the photoformation rates of ammonia and aldehydes from Cu(II)–amino acid complexes in an air-saturated solution increase slightly by 10–20% compared with those in deaerated solution. Although it is not known how the photoreactivity of amino acids with different side chains is affected if they are part of a larger macromolecule (e.g., algal component, cell membrane, or DOM), our results provide a useful starting point for studies in more complex systems.

In the presence of trace amounts of copper, the strong Cu(II)–DOM complexes can undergo redox transformations to form Cu(I) species and may cause the inhibition of the triplet excited state of DOM.<sup>37–39</sup> The indirect DOM-photosensitized degradation of dissolved free amino acids

may greatly reduce; on the other hand, the direct phototransformation of Cu(II)–amino acid complexes needs to be considered and may contribute to the bioavailable nitrogen for aquatic microorganisms and cause biological damage on cell surfaces in sunlit waters. Overall, this study provides further insight into the effect of side-chain structure on the direct phototransformation of Cu(II)–amino acid complexes and improves our assessment of the oxidative destruction of the copper-binding sites on DOM, cell, or algal surfaces in sunlit waters.

### 3. CONCLUSIONS

Our study reveals that the side-chain structure and the Cu(II) complex stoichiometry play an important role in the photolysis of Cu(II)–amino acid complexes. In deaerated solution, the Cu(I) quantum yields follow the trend of Ala > Val, Leu, Ile, and Phe > Gly > Met > Pro, which can be rationalized by considering the stability of the carbon-centered radicals and the efficient depopulation of the photoexcited state. The relative order of producing Cu(I) in deaerated solution parallels the one producing ammonia and aldehydes in deaerated or air-saturated solution. Therefore, the photoformation of Cu(I) in deaerated solution is a useful indicator to predict the photodegradation of amino acids when Cu(II)–amino acid species exist in natural waters.

### 4. EXPERIMENTAL SECTION

**4.1. Materials and Solution Preparation.** All of the ligands used were reagent or analytical grade and obtained from Fluka (Buchs, SG, Switzerland): >99% pure for glycine (Gly) and L-phenylalanine (Phe) and >99.5% pure for L-proline (Pro), L-methionine (Met), L-valine (Val), L-leucine (Leu), and L-isoleucine (Ile). 2,4-Dinitrophenylhydrazine (DNPH) (>97%) was obtained from Sigma (St. Louis, MO). Bathocuproine (sulfonated sodium salt) was from GFS. 2-Nitrobenzaldehyde (2-NB > 98%) was from Aldrich. Ultrapure water ( $\geq 18.2$  M $\Omega$ -cm resistivity) was generated by a Milli-Q water purification system (Millipore, Bedford, MA) for all solutions. Equilibrium concentrations of Cu(II)–amino acid complex species were computed using Visual MINTEQ 3.0 program.<sup>57,58</sup> Ionic strength corrections and equilibrium formation constants used for all inorganic Cu(II) species were taken into consideration and details of the methodologies used are described elsewhere.<sup>36</sup> The experimental solution conditions were optimized from calculations and summarized in Table S1.

**4.2. Analytical Equipment and Measurements.** Absorbance measurements were performed using a Varian Cary 50 Bio UV–vis spectrophotometer. Photochemical experiments and chemical actinometry were conducted in 5.00 cm quartz cuvettes (Spectrocell Inc.) using a monochromatic illumination system (Spectral Energy Corp.) with a high-pressure 200 W Hg–Xe lamp (Ushio UXM 200H) emitting at 313 nm instead of sunlight in the photochemical reaction experiments as described previously.<sup>36</sup> Spectrophotometric determination of Cu(I) was performed with the bathocuproine disulfonate (BCS) method based on the molar absorptivity of the Cu(I)–bathocuproine complex at 484 nm of  $1.24 \times 10^4$  M<sup>-1</sup>cm<sup>-1</sup>.<sup>46,59</sup> Ammonia was determined by purge-and-trap ion chromatography developed previously.<sup>60,61</sup> A modified HPLC–DNPH method was used to determine aldehydes in waters containing Cu(II) ion.<sup>62</sup> 2-

Nitrobenzaldehyde (2-NB) was chosen as an actinometer for the monochromatic illumination system with a quantum yield of  $0.41 \pm 0.02$  at 313 nm in an aqueous solution.<sup>63</sup> The measured experimental values of the volume-averaged incident actinic flux  $I_0$  at 313 nm were between 0.63 and 0.87  $\mu$ (einstein) L<sup>-1</sup> s<sup>-1</sup> for these experiments. All pH measurements were made using a Radiometer Analytical Ioncheck 45 meter combined with a glass electrode (Mettler Toledo Inlab 439/120). The pH electrode was calibrated periodically using NIST-traceable standard buffers (pH 4.00, 7.00, and 10.00). The apparent first-order rate constant ( $j_{i \rightarrow \text{Cu(I)}}$ , s<sup>-1</sup>) for the photoformation of Cu(I) from a given individual Cu(II) complex species in terrestrial sunlight was estimated by integrating eq 4 over the wavelength range  $290 < \lambda \leq 340$  nm

$$j_{i \rightarrow \text{Cu(I)}} = \int \{[\ln(10)][\Phi_{\text{Cu(I),i}}(\lambda)][\epsilon_{\text{Cu(II),i}}(\lambda)][I'(\lambda)]\} d\lambda \quad (4)$$

where values of  $I'(\lambda) d\lambda$  are published spherically integrated solar irradiance values over a specified wavelength range for a solar zenith angle of 30°, values of  $\epsilon_{\text{Cu(II),i}}(\lambda)$  were calculated from the measured absorption spectra  $290 < \lambda \leq 340$  nm, and values of  $\Phi_{\text{Cu(I),i}}(\lambda)$  were obtained from  $\Phi_{\text{Cu(I),i}}$  at 313 nm.<sup>35,64</sup> As a conservative estimate, it was assumed that  $\Phi_{\text{Cu(I),i}}(\lambda) = \Phi_{\text{Cu(I),i}}(313)$  for  $\lambda \leq 313$  nm and  $\Phi_{\text{Cu(I),i}}(\lambda) = \Phi_{\text{Cu(I),i}}(313) \cdot [\epsilon_i(\lambda)/\epsilon_i(313)]$  for  $313 < \lambda \leq 340$  nm.<sup>46</sup>

### ■ ASSOCIATED CONTENT

#### Supporting Information

The Supporting Information is available free of charge at <https://pubs.acs.org/doi/10.1021/acsomega.1c04277>.

Details of the experimental solution conditions used for this study (Table S1); the molar absorptivities and calculated equilibrium speciation for seven amino acid systems (Tables S2–S8); the quantum yields and calculated equilibrium speciation for seven amino acid systems (Table S9–S15); comparison of the measured and calculated molar absorptivities (Figure S1); and comparison of the measured and calculated photochemical parameters (Figure S2) (PDF)

### ■ AUTHOR INFORMATION

#### Corresponding Author

**Chien-Hou Wu** – Department of Biomedical Engineering and Environmental Sciences, National Tsing Hua University, Hsinchu 30013, Taiwan; Institute of Analytical and Environmental Sciences, National Tsing Hua University, Hsinchu 30013, Taiwan; [orcid.org/0000-0001-5243-2700](https://orcid.org/0000-0001-5243-2700); Phone: 886-3-5715131; Email: [chwu@mx.nthu.edu.tw](mailto:chwu@mx.nthu.edu.tw); Fax: 886-3-5718649

#### Authors

**Chen-Jui Lin** – Department of Biomedical Engineering and Environmental Sciences, National Tsing Hua University, Hsinchu 30013, Taiwan

**Po-Yen Wang** – Department of Civil Engineering, Widener University, Chester, Pennsylvania 19013, United States

**Yi-Liang Lin** – Department of Biomedical Engineering and Environmental Sciences, National Tsing Hua University, Hsinchu 30013, Taiwan

**Sheng-Te Chang** – Department of Biomedical Engineering and Environmental Sciences, National Tsing Hua University, Hsinchu 30013, Taiwan

Chao-Sheng Hsu – Department of Biomedical Engineering and Environmental Sciences, National Tsing Hua University, Hsinchu 30013, Taiwan

Shu-Pao Wu – Department of Applied Chemistry, National Yang Ming Chiao Tung University, Hsinchu 30010, Taiwan;  
orcid.org/0000-0002-4424-5486

Complete contact information is available at:  
<https://pubs.acs.org/10.1021/acsomega.1c04277>

## Notes

The authors declare no competing financial interest.

## ACKNOWLEDGMENTS

We are grateful to the anonymous reviewers for their kind and useful comments. This study was supported by the Ministry of Science and Technology of Taiwan (the Republic of China) under Grant Numbers: NSC 100-2113-M-007-004, NSC 101-2113-M-007-011, and MOST 103-2113-M-007-006.

## REFERENCES

- (1) Sýkora, J. Photochemistry of copper complexes and their environmental aspects. *Coord. Chem. Rev.* **1997**, *159*, 95–108.
- (2) Cieřla, P.; Kocot, P.; Mytych, P.; Stasicka, Z. Homogeneous photocatalysis by transition metal complexes in the environment. *J. Mol. Catal. A: Chem.* **2004**, *224*, 17–33.
- (3) Armadori, N.; Accorsi, G.; Cardinali, F.; Listorti, A. Photochemistry and Photophysics of Coordination Compounds: Copper. In *Photochemistry and Photophysics of Coordination Compounds I. Topics in Current Chemistry*; Balzani, V.; Campagna, S., Eds.; Springer: Berlin, Heidelberg, 2007; *280*, pp 69–115.
- (4) Jiang, Q.; Xiao, N.; Shi, P.; Zhu, Y.; Guo, Z. Design of artificial metallo-nucleases with oxidative mechanism. *Coord. Chem. Rev.* **2007**, *251*, 1951–1972.
- (5) Isaeva, E. I.; Gorbunova, V. V. Formation of copper-containing particles on the quartz surface as a result of the photolysis of copper(II) complexes with amino acids. *Russ. J. Gen. Chem.* **2017**, *87*, 2852–2857.
- (6) Ndungu, K.; Hurst, M. P.; Bruland, K. W. Comparison of copper speciation in estuarine water measured using analytical voltammetry and supported liquid membrane techniques. *Environ. Sci. Technol.* **2005**, *39*, 3166–3175.
- (7) Ndungu, K. Model predictions of copper speciation in coastal water compared to measurements by analytical voltammetry. *Environ. Sci. Technol.* **2012**, *46*, 7644–7652.
- (8) Craven, A. M.; Aiken, G. R.; Ryan, J. N. Copper(II) binding by dissolved organic matter: Importance of the copper-to-dissolved organic matter ratio and implications for the biotic ligand model. *Environ. Sci. Technol.* **2012**, *46*, 9948–9955.
- (9) Buck, K. N.; Moffett, J.; Barbeau, K. A.; Bundy, R. M.; Kondo, Y.; Wu, J. The organic complexation of iron and copper: An intercomparison of competitive ligand exchange-adsorptive cathodic stripping voltammetry (CLE-ACSV) techniques. *Limnol. Oceanogr. Methods* **2012**, *10*, 496–515.
- (10) Takamura-Enya, T.; Tokutake, M. Novel speciation analysis of copper in river water: Observation of soluble anionic copper-ligand complexes. *Limnology* **2016**, *17*, 117–125.
- (11) Wong, K. H.; Obata, H.; Kim, T.; Wakuta, Y.; Takeda, S. Distribution and speciation of copper and its relationship with FDOM in the East China Sea. *Mar. Chem.* **2019**, *212*, 96–107.
- (12) Buerge-Weirich, D.; Sulzberger, B. Formation of Cu(I) in estuarine and marine waters: application of a new solid-phase extraction method to measure Cu(I). *Environ. Sci. Technol.* **2004**, *38*, 1843–1848.
- (13) Kieber, R. J.; Skrabal, S. A.; Smith, C.; Willey, J. D. Redox speciation of copper in rainwater: Temporal variability and atmospheric deposition. *Environ. Sci. Technol.* **2004**, *38*, 3587–3594.
- (14) Witt, M. L. I.; Skrabal, S.; Kieber, R.; Willey, J. Photochemistry of Cu complexed with chromophoric dissolved organic matter: Implications for Cu speciation in rainwater. *J. Atmos. Chem.* **2007**, *58*, 89–109.
- (15) Zitoun, R.; Clearwater, S. J.; Hassler, C.; Thompson, K. J.; Albert, A.; Sander, S. G. Copper toxicity to blue mussel embryos (*Mytilus galloprovincialis*) The effect of natural dissolved organic matter on copper toxicity in estuarine waters. *Sci. Total Environ.* **2019**, *653*, 300–314.
- (16) Bushaw, K. L.; Zepp, R. G.; Tarr, M. A.; Schulz-Jander, D.; Bourbonniere, R. A.; Hodson, R. E.; Miller, W. L.; Bronk, D. A.; Moran, M. A. Photochemical release of biologically available nitrogen from aquatic dissolved organic matter. *Nature* **1996**, *381*, 404–407.
- (17) Tarr, M. A.; Wang, W.; Bianchi, T. S.; Engelhaupt, E. Mechanisms of ammonia and amino acid photoproduction from aquatic humic and colloidal matter. *Water Res.* **2001**, *35*, 3688–3696.
- (18) Matsumoto, K.; Uematsu, M. Free amino acids in marine aerosols over the western North Pacific Ocean. *Atmos. Environ.* **2005**, *39*, 2163–2170.
- (19) Vähätalo, A. V.; Zepp, R. G. Photochemical mineralization of dissolved organic nitrogen to ammonium in the Baltic Sea. *Environ. Sci. Technol.* **2005**, *39*, 6985–6992.
- (20) Kitidis, V.; Uher, G.; Upstill-Goddard, R. C.; Mantoura, R. F. C.; Spyres, G.; Woodward, E. M. S. Photochemical production of ammonium in the oligotrophic Cyprus Gyre (Eastern Mediterranean). *Biogeosciences* **2006**, *3*, 439–449.
- (21) Mandalakis, M.; Apostolaki, M.; Tziaras, T.; Polymenakou, P.; Stephanou, E. G. Free and combined amino acids in marine background atmospheric aerosols over the Eastern Mediterranean. *Atmos. Environ.* **2011**, *45*, 1003–1009.
- (22) Chu, C.; Lundeen, R. A.; Sander, M.; McNeill, K. Assessing the indirect photochemical transformation of dissolved combined amino acids through the use of systematically designed histidine-containing oligopeptides. *Environ. Sci. Technol.* **2015**, *49*, 12798–12807.
- (23) Vasilevich, R. S.; Beznosikov, V. A. Amino acid composition of humic substances in tundra soils. *Eurasian Soil Sci.* **2015**, *48*, 593–599.
- (24) Matos, J. T. V.; Duarte, R. M. B. O.; Duarte, A. C. Challenges in the identification and characterization of free amino acids and proteinaceous compounds in atmospheric aerosols: A critical review. *TrAC, Trends Anal. Chem.* **2016**, *75*, 97–107.
- (25) Morel, F. M. M.; Price, N. M. The biogeochemical cycles of trace metals in the oceans. *Science* **2003**, *300*, 944–947.
- (26) Hsu-Kim, H. Stability of metal–glutathione complexes during oxidation by hydrogen peroxide and Cu(II)-catalysis. *Environ. Sci. Technol.* **2007**, *41*, 2338–2342.
- (27) Zhang, G.; Liang, S.; Shi, X.; Han, X. Dissolved organic nitrogen bioavailability indicated by amino acids during a diatom to dinoflagellate bloom succession in the Changjiang River estuary and its adjacent shelf. *Mar. Chem.* **2015**, *176*, 83–95.
- (28) Boreen, A. L.; Edlund, B. L.; Cotner, J. B.; McNeill, K. Indirect photodegradation of dissolved free amino acids: The contribution of singlet oxygen and the differential reactivity of DOM from various sources. *Environ. Sci. Technol.* **2008**, *42*, 5492–5498.
- (29) Remucal, C. K.; McNeill, K. Photosensitized amino acid degradation in the presence of riboflavin and its derivatives. *Environ. Sci. Technol.* **2011**, *45*, 5230–5237.
- (30) Zhang, Y.; Zhang, R.; Li, S. L.; Mostofa, K. M. G.; Fu, X.; Ji, H.; Liu, W.; Sun, P. Photo-ammonification of low molecular weight dissolved organic nitrogen by direct and indirect photolysis. *Sci. Total Environ.* **2021**, *764*, No. 142930.
- (31) Ferraudi, G.; Muralidharan, S. Photochemical properties of copper complexes. *Coord. Chem. Rev.* **1981**, *36*, 45–88.
- (32) Natarajan, P.; Ferraudi, G. Photochemical properties of copper(II)-amino acid complexes. *Inorg. Chem.* **1981**, *20*, 3708–3712.
- (33) Namasivayam, C.; Natarajan, P. Photopolymerization reactions initiated by copper(II)-amino acid chelates: Investigation of the

initiating species by flash photolysis. *I. J. Polym. Sci.: Polym. Chem. Ed.* **1983**, *21*, 1371–1384.

(34) Das, S.; Johnson, G. R. A.; Nazhat, N. B.; Saadalla-Nazhat, R. Ligand decomposition in the photolysis of copper(II)-amino-acid complexes in aqueous solution. *J. Chem. Soc., Faraday Trans. I* **1984**, *80*, 2759–2766.

(35) Faust, B. C. Aquatic Photochemical Reactions in Atmospheric, Surface, and Marine Waters: Influences of Oxidant Formation and Pollutant Degradation. In *Environmental Photochemistry. The Handbook of Environmental Chemistry*; Boule, P., Ed.; Springer-Verlag: Berlin, Heidelberg, 1999; Vol. 2, Part L, pp 101–122.

(36) Lin, C. J.; Hsu, C. S.; Wang, P. Y.; Lin, Y. L.; Lo, Y. S.; Wu, C. H. Photochemical redox reactions of copper(II)-alanine complexes in aqueous solutions. *Inorg. Chem.* **2014**, *53*, 4934–4943.

(37) Pan, Y.; Garg, S.; Waite, T. D.; Yang, X. Copper inhibition of triplet-induced reactions involving natural organic matter. *Environ. Sci. Technol.* **2018**, *52*, 2742–2750.

(38) Wan, D.; Sharma, V. K.; Liu, L.; Zuo, Y.; Chen, Y. Mechanistic insight into the effect of metal ions on photogeneration of reactive species from dissolved organic matter. *Environ. Sci. Technol.* **2019**, *53*, 5778–5786.

(39) Pan, Y.; Ruan, X.; Garg, S.; Waite, T. D.; Lei, Y.; Yang, X. Copper inhibition of triplet-sensitized phototransformation of phenolic and amine contaminants. *Environ. Sci. Technol.* **2020**, *54*, 9980–9989.

(40) Subramanian, G.; Prakash, H. Photo augmented copper-based Fenton disinfection under visible LED light and natural sunlight irradiation. *Water Res.* **2021**, *190*, No. 116719.

(41) Smith, R. M.; Martell, A. E. *Critical Stability Constants*; Plenum: New York, 1976–1989; pp 1–6.

(42) Martell, A. E.; Smith, R. M.; Motekaitis, R. J. *NIST Standard Reference Database 46: NIST Critically Selected Stability Constants of Metal Complexes, Version 7.0*; NIST: Gaithersburg, MD, 2003.

(43) Faust, B. C. Experimental determination of molar absorptivities and quantum yields for individual complexes of a labile metal in dilution solution. *Environ. Sci. Technol.* **1996**, *30*, 1919–1922.

(44) Solomon, E. I. Spectroscopic methods in bioinorganic chemistry: Blue to green to red copper sites. *Inorg. Chem.* **2006**, *45*, 8012–8025.

(45) Koebke, K. J.; Alfaro, V. S.; Pinter, T. B. J.; Deb, A.; Lehnert, N.; Tard, C.; Penner-Hahn, J. E.; Pecoraro, V. L. Traversing the red-green-blue color spectrum in rationally designed cupredoxins. *J. Am. Chem. Soc.* **2020**, *142*, 15282–15294.

(46) Sun, L.; Wu, C. H.; Faust, B. C. Photochemical redox reactions of inner-sphere copper(II)-dicarboxylate complexes: Effects of the dicarboxylate ligand structure on copper(I) quantum yields. *J. Phys. Chem. A* **1998**, *102*, 8664–8672.

(47) Wu, C. H.; Sun, L.; Faust, B. C. Photochemical formation of copper(I) from copper(II)-dicarboxylate complexes: Effects of outer-sphere versus inner-sphere coordination and of quenching by malonate. *J. Phys. Chem. A* **2000**, *104*, 4989–4996.

(48) Goodman, B. A.; McPhail, D. B.; Powell, H. K. J. Electron spin resonance study of copper(II)-amino-acid complexes: Evidence for cis and trans isomers and the structures of copper(II)-histidinate complexes in aqueous solution. *J. Chem. Soc., Dalton Trans.* **1981**, 822–827.

(49) Bukharov, M. S.; Shtyrlin, V. G.; Mukhtarov, A. S.; Mamin, G. V.; Stapf, S.; Mattea, C.; Krutikov, A. A.; Ilin, A. N.; Serov, N. Y. Study of structural and dynamic characteristics of copper(II) amino acid complexes in solutions by combined EPR and NMR relaxation methods. *Phys. Chem. Chem. Phys.* **2014**, *16*, 9411–9421.

(50) Poutsma, M. L. The radical stabilization energy of a substituted carbon-centered free radical depends on both the functionality of the substituent and the ordinality of the radical. *J. Org. Chem.* **2011**, *76*, 270–276.

(51) Hioe, J.; Zipse, H. Radical Stability—Thermochemical Aspects. In *Encyclopedia of Radicals in Chemistry, Biology and Materials, Vol. 1, Basic Concepts and Methodologies*; Chatgililoglu, C.; Studer, A., Eds.; John Wiley & Sons: Chichester, UK, 2012; pp 449–476.

(52) Zipse, H. Radical Stability—A Theoretical Perspective. In *Radicals in Synthesis I. Topics in Current Chemistry*; Gansauer, A., Ed.; Springer: Berlin, Heidelberg, 2006; *263*, pp 163–189.

(53) Hioe, J.; Zipse, H. Radical stability and its role in synthesis and catalysis. *Org. Biomol. Chem.* **2010**, *8*, 3609–3617.

(54) Luo, Y. R. *Comprehensive Handbook of Chemical Bond Energies*; CRC Press: Boca Raton, FL, 2007.

(55) Lundeen, R. A.; Janssen, E. M. L.; Chu, C.; McNeill, K. Environmental photochemistry of amino acids, peptides and proteins. *Chimia* **2014**, *68*, 812–817.

(56) Sharma, V. K.; Millero, F. J. Oxidation of copper(II) in seawater. *Environ. Sci. Technol.* **1988**, *22*, 768–771.

(57) Gustafsson, J. P. *MINTEQA2 version 4.0 and Visual MINTEQ version 3.0*; Department of Land and Water Resources Engineering, Royal Institute of Technology (KTH): Stockholm, Sweden, 2012.

(58) Allison, J. D.; Brown, D. S.; Novo-Gradac, K. J. *MINTEQA2/PRODEFA2, A Geochemical Assessment Model for Environmental Systems. Version 4.0*; EPA/600/3-91/021; U.S. Environmental Protection Agency: Athens, GA, 1999.

(59) Lomozová, Z.; Catapano, M. C.; Hrubša, M.; Karličková, J.; Macáková, K.; Kučera, R.; Mladěnka, P. Chelation of iron and copper by quercetin B-ring methyl metabolites, isorhamnetin and tamarixetin, and their effect on metal-based Fenton chemistry. *J. Agric. Food Chem.* **2021**, *69*, 5926–5937.

(60) Wang, P. Y.; Wu, J. Y.; Chen, H. J.; Lin, T. Y.; Wu, C. H. Purge-and-trap ion chromatography for the determination of trace ammonium ion in high-salinity water samples. *J. Chromatogr. A* **2008**, *1188*, 69–74.

(61) Lin, T. Y.; Pan, Y. T.; Lee, H. Y.; Wang, P. Y.; Wu, C. H. Markedly enhanced purge-and-trap performance and efficiency for the determination of ammonium ion in high-salinity water samples. *J. Chin. Chem. Soc.* **2012**, *59*, 718–726.

(62) Lin, Y. L.; Wang, P. Y.; Hsieh, L. L.; Ku, K. H.; Yeh, Y. T.; Wu, C. H. Determination of linear aliphatic aldehydes in heavy metal containing waters by high-performance liquid chromatography using 2,4-dinitrophenylhydrazine derivatization. *J. Chromatogr. A* **2009**, *1216*, 6377–6381.

(63) Galbavy, E. S.; Ram, K.; Anastasio, C. 2-Nitrobenzaldehyde as a chemical actinometer for solution and ice photochemistry. *J. Photochem. Photobiol., A* **2010**, *209*, 186–192.

(64) Leifer, A. *The Kinetics of Environmental Aquatic Photochemistry: Theory and Practice*; ACS Professional Reference Book, American Chemical Society: Washington, DC, 1988.